EXPLAINABLE MACHINE LEARNING FOR SOILCRETE UCS PREDICTIONS

Katherine Cheng, University of California, Davis, CA, USA, +1 (530) 752-0586, katcheng@ucdavis.edu
James R. Gingery, Keller North America, Inc., Irvine, CA, USA
Martin D. Yossifov, University of California, Davis, CA, USA
Katerina Ziotopoulou, University of California, Davis, CA, USA

ABSTRACT

Soil mixing is a ground improvement method that consists of mixing cementitious binders with soil in-situ to create soilcrete. A key parameter in the design and construction of this method is the Unconfined Compressive Strength (UCS) of the soilcrete after a given curing time. This paper explores the intersection of Machine Learning (ML) with geotechnical engineering and soilcrete applications. A database of soilcrete UCS and site/soil/means/methods metadata is compiled from recent projects in the western United States and leveraged to explore UCS prediction with the eXtreme Gradient Boosting (XGBoost) ML algorithm which resulted in a ML model with a R^2 value of 88%. To achieve insights from the ML model, the Explainable ML model SHapley Additive exPlanations (SHAP) was then applied to the XGBoost model to explain variable importances and influences for the final UCS prediction value. From this ML application, a blueprint of how to scaffold, feature engineer, and prepare soilcrete data for ML is showcased. Furthermore, the insights obtained from the SHAP model can be further pursued in traditional geotechnical research approaches to expand soil mixing knowledge.

Keywords: machine learning, unconfined compressive strength, explainable machine learning, soil mix, soilcrete, XGBoost, SHAP

INTRODUCTION

Soil mixing is a ground improvement method that consists of mixing cementitious binders with in-situ soil to create soilcrete. This treatment is utilized to treat liquefiable soils (e.g., Martin et al. 2004, Boulanger and Shao 2021, Cao et al. 2023), improve soft or compressible ground (e.g., Filz et al. 2012, Frikha et al. 2017), serve as slope protection (e.g., Kitazume and Maruyama 2007, Jamsawang et al. 2016), and has many more applications listed in Bruce et al. (1998). A key parameter in this technique's design and construction is the Unconfined Compressive Strength (UCS) of the resulting soilcrete after a specified curing time. However, estimating UCS can be challenging due to the numerous factors influencing the results, including soil type, soil moisture content, binder content, soil chemistry, soil heterogeneity, and mixing means and methods. In current North American design-build practice, pre-construction UCS design values are typically qualitatively estimated based on contractors' experience although research has explored relationships between UCS and various factors such as porosity (e.g., Pham et al. 2021, Amrioui et al. 2023), water/cement ratio (e.g., Filz et al. 2012, Pham et al. 2021, Karpisz et al. 2018), soil type (e.g., Szymkiewicz et al. 2015, Karpisz et al. 2018) amongst many others. In design guides, there are existing guidelines and strength correlations in North America such as from the FHWA (Bruce et al. 2013) with further overview of global practices in Bruce et al. (1998). Existing correlations may not be suitable for current applications because of recent advances in deep mixing equipment and methodologies. There is a need for more rational and quantitative estimates of UCS for use in pre-construction design analyses.

This paper investigates the application of the XGBoost Machine Learning (ML) algorithm, coupled with explainable ML SHAP (Shapley Additive exPlanations), on a soilcrete dataset from western U.S. projects performed by Keller North America, Inc. following the ML model pipeline shown in Fig. 1. The work presented uses a dataset comprised of 2226 data points from 15 jobsites to fit the final XGBoost model.

The feature engineering and hyperparameter tuning processes for building the ML model are demonstrated and established. The trained XGBoost model is then presented along with SHAP results, which are subsequently evaluated and explained at the global and local level. The paper concludes with lessons learned from the UCS data through the application of SHAP on the XGBoost algorithm and the potential usage of SHAP in future ground improvement ML application work.

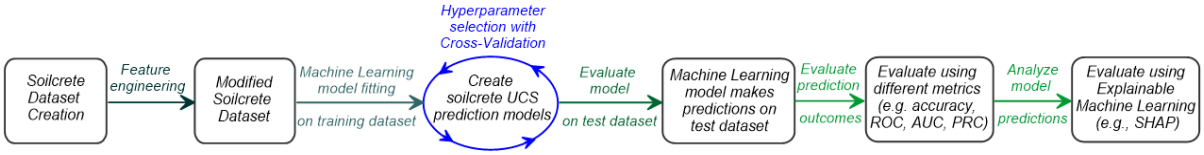

Fig. 1. ML model pipeline for UCS prediction

DATASET AND FEATURE ENGINEERING

The dataset is composed of UCS break data from 15 different soil mixing projects from Sept. 2020 to March 2023 (a 904-day timespan). All data processing was done in Python by combining data acquisition (DAQ) reports, geotechnical site report data, UCS break data, and site cone penetration test (CPT) data to result in a dataset of 2,328 points total. To extract the closest site CPT data to the tested soilcrete column location, as-built plans were reviewed and the closest CPT by distance was assigned to the soilcrete column location. As grout is injected in the mixing process, soilcrete is displaced upward. CPT depth data was adjusted to account for the grout injection so that UCS sample depths aligned with the corresponding CPT data depths. To account for the homogenization effect of a soil profile from the passage of the soil mixing tool, the soil properties were averaged across a 5 ft (1.5 m) vertical interval around the original location pre-ground improvement. Soil I_c was calculated via Robertson (2010) while CPT properties were extracted from the site CPT data.

Ground improvement designs typically specify a minimum 28-day strength, either as an average value or a certain percentile passing value. Although the dataset initially included UCS results at the 56-day mark, these data were sparse and appeared to be biased toward lower values. Therefore, any UCS tests conducted beyond the 35-day mark were excluded from the analysis. This resulted in 2226 datapoints, with most of the UCS tests results being from 7-day (23%), 14-day (24%), and 28-day (36%) tests. None of the data were scaled or rebalanced, as XGBoost, being a nonparametric decision tree-based ML algorithm, does not require either of these transformations.

Further summary statistics are listed in Table 1, where the distribution of each feature can be seen. Other features presented are the binder content, Blade Rotation Number (BRN) (based on Bruce et al. 2013), CPT sleeve friction (f_s), CPT tip resistance (q_c), and grout specific gravity. There are two project time-series features: "Days from First Project Column" and "Days from Earliest Dataset Column". "Days from First Project Column" refers to the timespan between the start of the project and the time the tested column was installed. "Days from Earliest Dataset Column" refers to the timespan from the very first soil column date in the entire dataset to the installation date of the soilcrete datapoint in question (hence it spans from 0 to 904 days). These two time-based features are intended to track UCS changes within an individual project timespan and over the entire dataset's timespan, respectively.

There are two sampling techniques used to retrieve soilcrete for UCS testing: core (indicated with a 0 in the dataset) or grab (indicated with a 1 in the dataset). Grab samples are retrieved using a trap door bucket that is lowered to the target depth in a freshly mixed wet column. The wet soilcrete is then cast into cylinders and cured in a humidity- and temperature-controlled environment prior to UCS testing. Core sampling uses a core barrel to retrieve samples from cured soilcrete. Specimens are selected from the

cores, sealed, and cured in a controlled environment until they are tested at 28 days. Target depths are typically dispersed along the intact core sections and several depths from one core can be tested.

Table 1: Summary statistics for both categorical and numerical variables

Total count	2226
Timespan (days)	904
Number of jobsites	15

Soilcrete Sample Type	**Counts**
0 (core)	1882
1 (grab)	344

	Age of Specimen (days)	**Binder Content (kg/m^3)**	**BRN**	**CPT fs (tsf)**	**CPT qc (tsf)**	**Days from First Project Column**	**Grout Specific Gravity**	**Soil Ic**	**UCS (psi)**
Mean	16.5	204.3	736.1	1.1	59.1	18.8	1.4	2.5	297.7
Std	9.6	29.6	287.6	1.1	51.9	19.4	0.0	0.5	126.9
Min	2	141.2	0	0.03	3.6	0	1.3	1.4	39
Median	14	200	660.2	0.9	40.6	14	1.4	2.4	280
Max	32	377.3	2407.1	10.5	317.9	97	1.6	3.9	970

XGBOOST ALGORITHM & TRAINING

The ML algorithm chosen to predict the UCS is the XGBoost algorithm implemented in Python (Chen and Guestrin 2016) with cross-validation and accuracy evaluation from Scikit-learn (Pedregosa et al. 2011). The XGBoost algorithm is a variation of gradient boosting ensemble algorithms, which consists of multiple decision trees that add upon one another to minimize the residual between the predicted and true values. The first decision tree in an XGBoost ensemble formulates a prediction by using the supplied predictor variables and recursively dividing the dataset into groups based on input features. The next decision trees to be added to the XGBoost algorithm instead predict on the residuals from the difference (residuals) between the previous prediction and the true value as the new target. These decision trees based on incremental residuals are then added onto the overall XGBoost ensemble tree algorithm, with multiple trees being built each iteration and only the optimal decision tree based on the given loss function (in this case, mean squared error (MSE)) is kept. The chain of decision trees continues until further decision tree growth does not significantly improve overall accuracy or max tree depth has been reached.

The XGBoost implementation by Chen and Guestrin (2016) features optimized computation paths and regularization to prevent overfitting. Furthermore, the nonparametric XGBoost algorithm has been shown to perform better on small datasets than other ML algorithms (Nenchev et al. 2022, Zou et al. 2022). As the UCS dataset is relatively small and is neither linearly nor normally-distributed, the nonparametric XGBoost is an appropriate algorithm for this ML application. Attempts to fit the dataset with linear-based algorithms (e.g., linear regression, Support Vector Regression (SVR))–even with transformed and scaled data–did not perform satisfactorily in terms of accuracy and residual plot patterns.

In the fitting process of the XGBoost algorithm, several hyperparameters are specified before training, such as: the number of decision trees (n_estimators), L1 regularization on weights (alpha), L2 regularization on weights (lambda), number of features selected per decision tree (colsample_bytree), boosting step size (eta), minimum sum of weights in a decision tree leaf (min_child_weight), subsample of training set to be used per decision tree (subsample), minimum loss reduction for splitting further in a decision tree (gamma). All these hyperparameters were utilized in the hyperparameter search to prevent ML model overfitting (when the ML model overly memorizes the training data information and subsequently performs poorly when exposed to unseen testing data).

The dataset was randomly split into two portions with 80% of it for training and 20% of it for testing. To improve the performance of the XGBoost algorithm the hyperparameters were optimized via a random hyperparameter grid search with five-fold cross-validation (CV) run on the training set over a wide range

of hyperparameter values to further prevent overfitting. The final hyperparameter values are: number of decision trees (810), L1 regularization on weights (0), L2 regularization on weights (0.5), number of features selected per decision tree (0.5), boosting step size (0.3), minimum sum of weights in a decision tree leaf (1), subsample of training set to be used per decision tree (0.8), minimum loss reduction for splitting further in a decision tree (0). The rest of the hyperparameters used for XGBoost were kept as default.

EXPLAINABLE ML (SHAP) ALGORITHM

SHAP (Lundberg and Lee 2017) allows ML models to achieve both accuracy and interpretability. SHAP works as a wrapper around the original ML model, probing the ML model to calculate the contributions and interactions of the input features on the final prediction and can be applied to most ML models. The background of this technique originates from game theory as an additive feature attribution method, meaning the predicted output is a linear combination of the input features as showcased in Equation 1.

$$g(z') = \phi_0 + \sum_{i=1}^{M} \phi_i z'_i \qquad (1)$$

where $z' \in 0,1^M$*, M is the number of simplified input features, and* $\phi_i \in R$ (Lundberg and Lee 2017)

SHAP values are to satisfy three criteria: 1) Local accuracy: The explanation model output should match that of the original ML model. 2) Missingness: If a feature value is 0, then it should reflect as such in the explanation model as a 0 for the influence value. 3) Consistency: The explanation model should consistently reflect any changes as the ML model changes. A unique solution has been proven to satisfy these three criteria as Equation 2.

$$\phi_i(f, x) = \sum_{z' \subseteq x'} \frac{|z'|!(M-|z'|-1)!}{M!} [f_x(z') - f_x(z' \backslash i)] \qquad (2)$$

where $|z'|$ *is the number of non-zero entries in* z'*, and* $z' \subseteq x'$ *represents all* z' *vectors where the non-zero entries are a subset of the non-zero entries in* x' (Lundberg and Lee 2017)

As Equation 2 is computationally intensive to solve, there are approximation SHAP algorithms, such as KernelSHAP and TreeSHAP. This paper utilizes TreeSHAP as it is designed for tree-based algorithms, such as XGBoost, and efficiently calculates SHAP values for all input features. Utilizing SHAP allows us to explore model biases, outlier effects, and trends within input feature values that can hint towards their overall influence on the model.

XGBOOST & SHAP RESULTS

The final XGBoost model has an R^2 of 88% on the test set, indicating that 88% of the variance of the target variable (UCS) is explained by the variance of the input parameters in this model. Fig. 2 showcases the fit of the predicted vs. true values of the test set along with the projected 1:1 line. As the points fall around the 1:1 line, the fit is reasonable, attesting to the high R^2 value. To extract further insights, SHAP was then applied onto the XGBoost model.

The SHAP feature importance plot in Fig. 3 showcases the proportional impact of each feature on predicting for the final UCS value. The features on the y-axis are ordered from the most to least influential. As expected from literature, specimen age is shown as the most influential input feature as it has the largest bar in Fig. 3. The time series variable of days since earliest dataset column is the second most influential, indicating a change in overall UCS values over the years. The other features are within the same magnitudes of influence, with sample type being the least influential out of all of them.

Looking further into the influence of individual features, the SHAP global summary plots in Fig. 4a and 4b provide an expanded perspective beyond the SHAP feature importance plot (Fig. 3), highlighting previously obscured trends. The y-axis arranges input features according to their respective influence, with the most impactful input feature positioned at the top and the least influential at the bottom. In these plots, the color of each data point signifies the feature value, with red indicating a high value (e.g., 5) and blue a low value (e.g., 0) relative to the internal range of each feature. When selecting a specific feature value, the corresponding x-axis value indicates the resulting change in the final predicted UCS value, either increasing (towards the right) or decreasing (towards the left). This change in predicted UCS values due to inputting feature values always builds on the expected UCS value of 297 psi (2.05 MPa) or the initial XGBoost model bias. This expected value stems from the final prediction of all feature values with a SHAP value of 0 (the center of the x-axis) and indicates the default assumption for a starting UCS prediction that has no further input information.

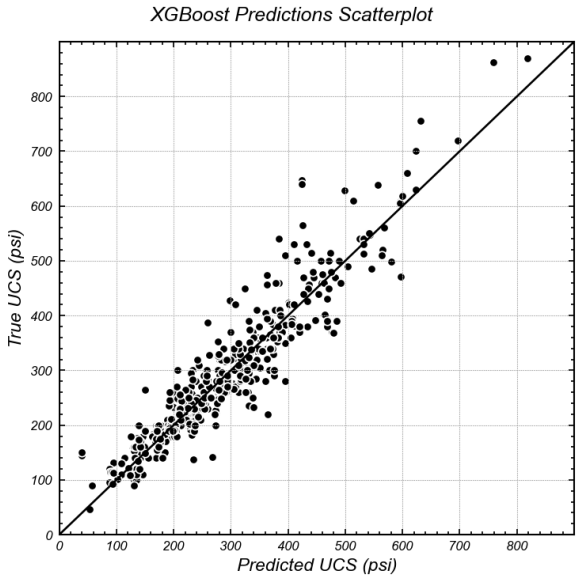

Fig. 2. Predicted vs True UCS with a 1:1 line.

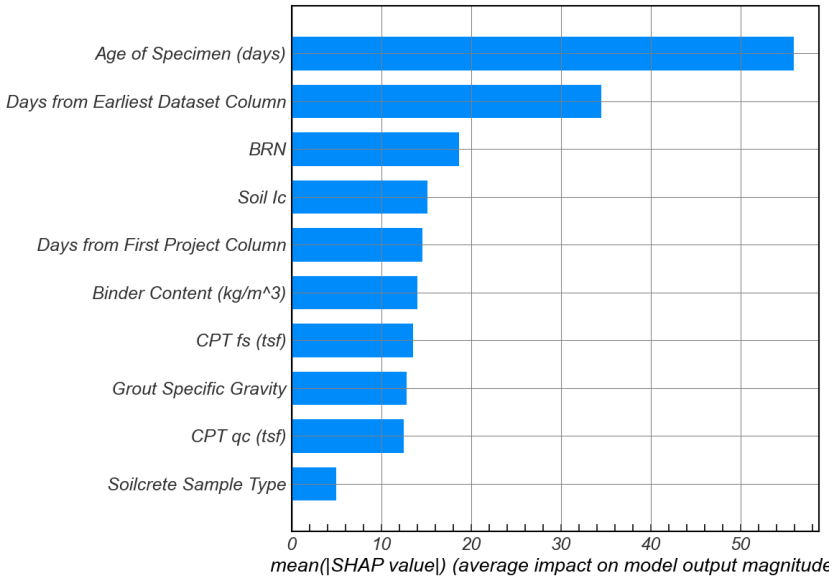

Fig. 3. SHAP feature importance plot, explanation in text.

Two SHAP global summary plots are presented: one for the training dataset (Fig. 4a) and the other for the testing dataset (Fig. 4b). Since SHAP aims to elucidate the workings of the XGBoost model, understanding the model's behavior during training versus testing provides valuable insights. These trends observed from the SHAP values apply to this dataset and model, however, generalizable insights and model validation can be gained through this approach. Figure 4 shows that in general specimen age can now be further parsed into three general clusters. These clusters follow the three main test ages of 7 days (blue), 14 days (purple), and 28 days (red) and contribute negatively, neutrally, and positively to the base expected UCS predicted value. This aligns with established trends documented in the literature (e.g., Bruce et al. 2013), wherein an increase in specimen age correlates with a corresponding increase in UCS value.

For the "Days from Earliest Dataset Column" feature, the SHAP value decreases as the count of days increases. Due to it being a time-based variable that increases with each passing day in the dataset, this indicates a decrease in predicted UCS over time. However, the specified minimum UCS values were achieved for all the projects in the database. The authors believe the decrease may reflect more accurate targeting of design strengths over time, which reduces the more conservative early mix designs that overshot the required/target UCS. Additionally, this phenomenon also occurs in the other time-series feature of "Days from First Project Column". High feature values result in lower SHAP values, indicating a drop in UCS throughout a project installation. This reflects the typical adjustment period in a project of starting with a high binder content that often overshoots the design UCS, then over time reducing the binder content to achieve lower UCS closer to the specified design strength.

Another concern for soilcrete mix design is the soil type itself, which was identified in the dataset by the predominant I_c in the sampled section. The soil type I_c SHAP values reflect an increase in sand-like soil (low I_c) and decreasing in clay-like soil (high I_c). Additionally, an increase in grout specific gravity directly contributes to an increase in predicted UCS value according to the SHAP values in Fig. 4a and 4b. Of note is the influence of sampling method on the resultant UCS value. Most of the non-neutral values in the SHAP cluster for soilcrete sample type are that of the core samples (indicated by their low feature value of 0/blue). Therefore, a core sample could increase the predicted strength by up to 90 psi (0.62 MPa). This observation is most pronounced in Fig. 4a. However, it has the least effect on the predicted UCS value out of all the features as it is lowest on the feature importance plot.

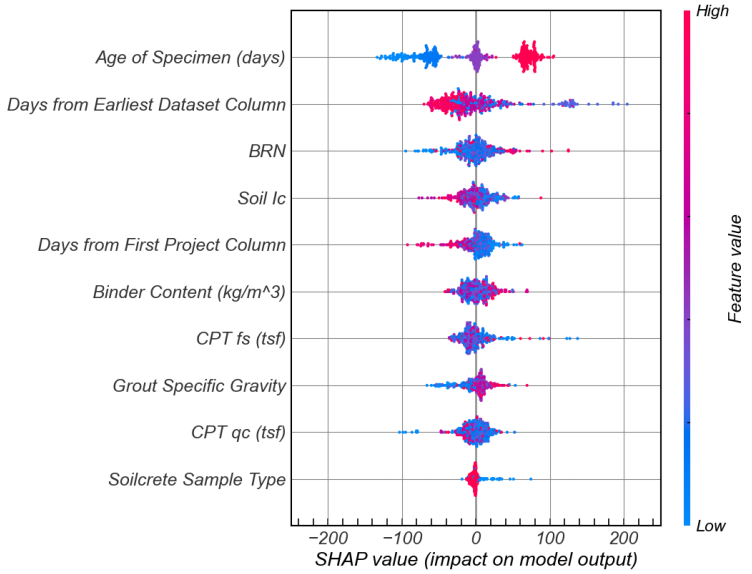

Fig. 4a. SHAP global summary plot for test set, explanation in text.

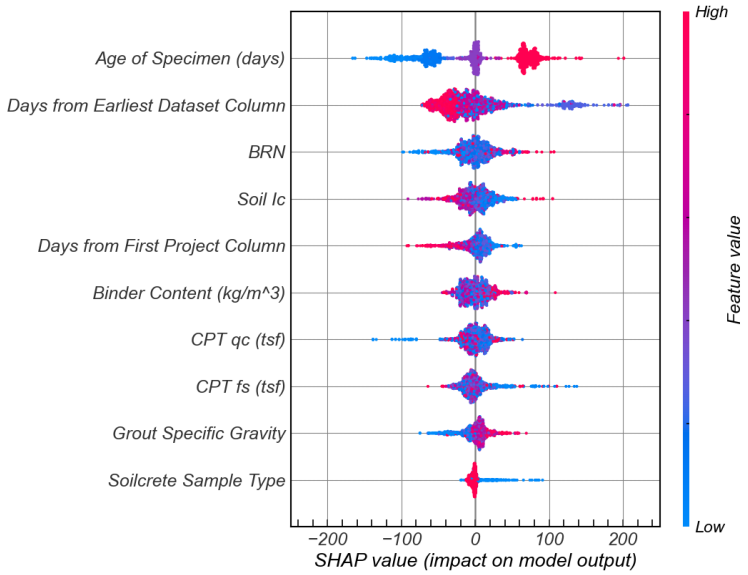

Fig. 4b. SHAP global summary plot for train set, explanation in text.

To further examine the details of the XGBoost model behavior, SHAP plots for individual datapoint predictions can be generated. Before selecting the datapoints to be observed, a general overview of the datapoint spread is created in Fig. 5, a boxplot of the true UCS values from the test set. Fig. 6, 7, and 8 are the individual SHAP plots corresponding to points A, B, and C, respectively. The points were picked to encompass a variety of cases: A) a typical case where the bulk of the test UCS values are, B) the test case with the largest residual, C) the test case of the greatest outlier value.

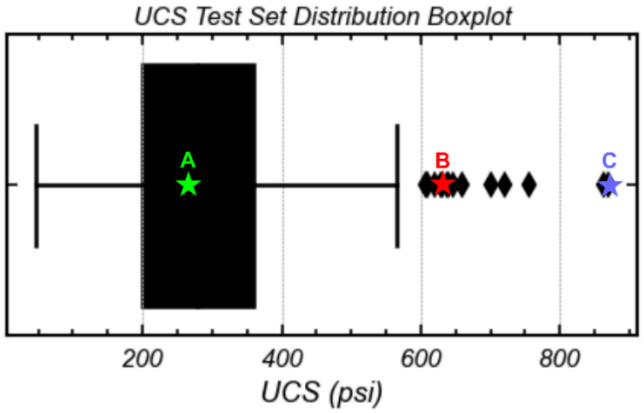

Fig. 5. Distribution of XGBoost test set UCS values

Each of these individual datapoint SHAP plots start on the expected value of 297 psi (2.05 MPa), shown by the line marked as the “base value”. Then, subsequent input features are added on, with the impact per feature value based on the global SHAP value calculations (Fig. 4). Positively contributing features are red while negatively impacting features are blue. Subsequent adding and subtracting from the base value continues until all feature values for the given datapoint have been added in. The final value in bold on the stacked plot is the final predicted UCS value, with the width of each feature’s bar indicating the magnitude of impact the feature had positively or negatively.

For point A (Fig. 6), the true value is 273 psi (1.88 MPa) and the predicted value is also 273 psi (1.88 MPa). The large positively contributing features were the specimen age of 17 days and silty sand soil. The BRN and the soil mix being installed on the 16th day of the project were also positively contributing, but from the widths of the stacked plot, they were not as influential as the previously mentioned features. The negatively contributing features were a low CPT f_s, average binder content, and the soil mix being installed 68 days into the dataset's overall timeline. Less important features that negatively contributed are the CPT q_c and the soilcrete sample type, but the contributions are negligible, on the order of less than 5 psi (0.034 MPa). The predicted UCS value is highly accurate, showing the XGBoost model has learned the pattern relatively well for the region where most of the test data is clustered.

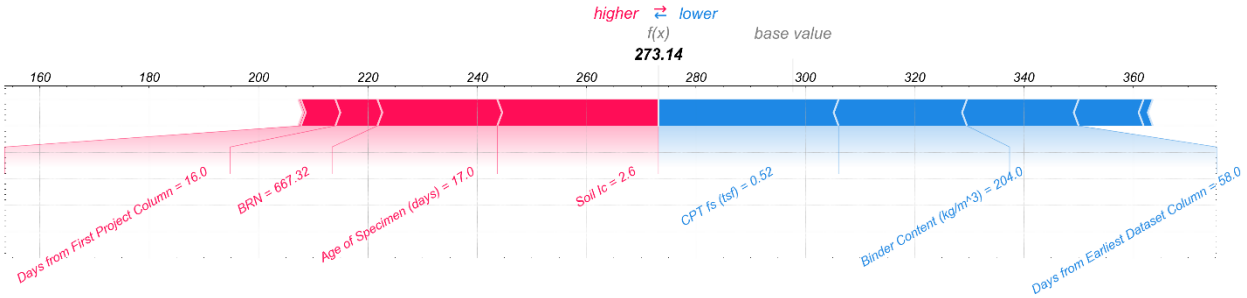

Fig. 6. SHAP plots for datapoint A, typical correct prediction: True value is 273 psi (1.88 MPa).

The test case with the greatest residual is Fig. 7, point B, where the true value is 647 psi (4.46 MPa) and the predicted value is 425 psi (2.93 MPa). This is a case of underprediction and the SHAP local plot reveals the CPT q_c and the days from first project column values as the negatively impacting variables. From this result, a closer inspection of the CPT q_c data could be performed to understand whether the sampled soil mix was correlated to the correct CPT. This is an example of SHAP helping identify errors or gaps from the initial dataset that the XGBoost model may have inadvertently learned.

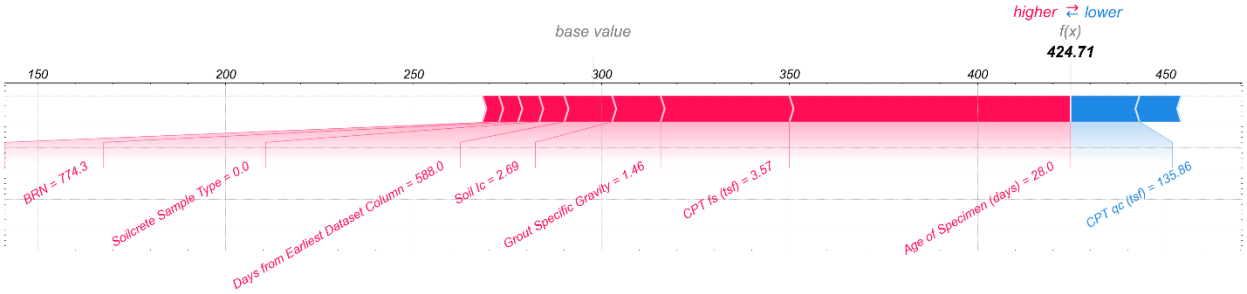

Fig. 7. SHAP plots for datapoint B, largest residual datapoint: True value is 647 psi (4.46 MPa).

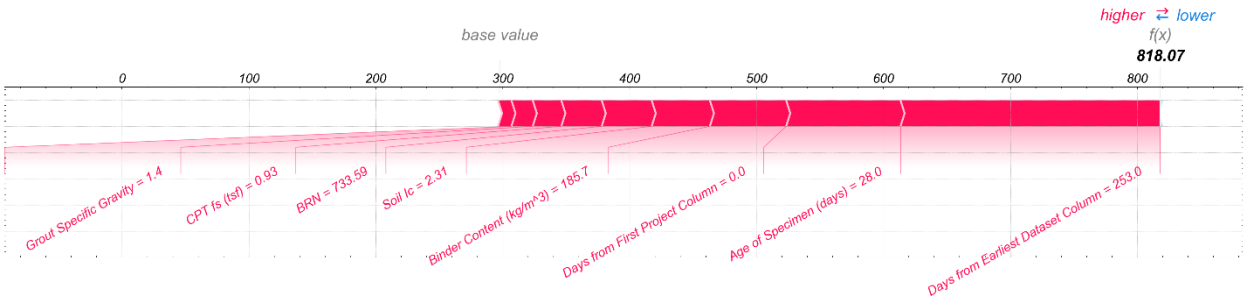

Fig. 8. SHAP plots for datapoint C, highest UCS value in test dataset: True value is 870 psi (6.0 MPa).

The highest UCS true value test case is Fig. 8, point C, where the true value is 870 psi (6.0 MPa) and the predicted value is 818 psi (5.64 MPa). The local SHAP plot reveals that all variables were calculated as positively contributing to the final predicted UCS value. This indicates that XGBoost can predict values of outliers in the dataset in a non-random manner, having learned that each of these features is a positive increase upon the base UCS value.

CONCLUSIONS

Given the complex nonlinear relationships between soilcrete's UCS with the various chosen input features, the ML algorithm XGBoost was chosen for its capability to handle nonlinearity, nonparametric data, and small dataset sizes. To enhance interpretability, Explainable ML (SHAP) was applied to the fitted XGBoost regression model to predict soilcrete UCS data from a dataset consisting of 2226 points post-feature engineering from 15 soil mixing projects in the western U.S.. The XGBoost model achieved a R^2 value of 88%, then SHAP was further applied to explain the internal prediction patterns learned from the dataset. Key observations from SHAP are: 1) age emerges as the most influential variable, with greater age corresponding to higher predicted UCS values; 2) predicted UCS values tend to decrease over time, both across the overall dataset timescale and within individual project timescales. This is attributed to reduced conservatism in design and adjustments in binder contents over time; 3) soil type plays a significant role, with clay-like soils generally exhibiting lower predicted UCS compared to sand-like soils; 4) while sampling method minimally impacts overall predictions, core samples tend to contribute slightly higher UCS values compared to sand wet grab samples.

This initial exploration with SHAP showcases how previously black-box ML models (e.g., XGBoost) can gain mathematically backed explanations, with resultant insights that match those known from literature. As shown in the observation on the global dataset SHAP plots, SHAP can identify existing bias in the original ML model along with what constitutes as the feature values for the default predictions. From there, SHAP can identify which are the most important predictive features (e.g., Age, BRN) and which values within the features are influential (e.g., high I_c values (clay) contribute to lower UCS). These identified features can be compared to what is known from literature to verify the ML algorithm is learning properly. This can also lead to further work implementing field tests targeting the effects of any novel variable trends and values identified via SHAP value patterns. From the local datapoint SHAP plots, the extent of the XGBoost model abilities can be parsed and areas to be improved on can be identified. With this knowledge, targeted field sampling can be implemented in a non-random manner to fill in any identified dataset gaps to further bolster the XGBoost model.

The final XGBoost model shows potential as a tool for knowledge gain, showcasing that the ML model can learn the same patterns from features as soilcrete strength literature indicates. This inspires confidence in the ability to apply ML to this complex challenge and can lead to future research avenues for understanding the components of soilcrete UCS. Future work will explore additional input features (e.g., Friction Ratio), or transforming input features (e.g., standardizing UCS against age). Furthermore, feature interactions can be explored with SHAP to see if combining certain values of features may lead to different effects than if independently input into the ML model.

ACKNOWLEDGMENTS

The authors acknowledge Miguel Diaz (Keller) for helping organize the data sources, and Dr. Tanner Blackburn (Keller) and Dr. Brian Freilich (Keller) for their insightful comments in the research process. This material is based upon work primarily supported by Keller North America. Any opinions, findings and conclusions, or recommendations expressed in this material are those of the authors and do not necessarily reflect those of Keller North America.

REFERENCES

Amrioui, J., Le Kouby, A., Duc, M., Guedon, J.-S., & Lansac, F. (2023). Relationship between porosity and water permeability for deep soil mixing material. International Journal of Geomechanics, 23(7), 04023086.

Boulanger, R. W., & Shao, L. (2021). Liquefaction mitigation with deep mixing.

Bruce, D. A., Bruce, M. E. C., & DiMillio, A. F. (1998). Deep mixing method: A global perspective. Geotechnical Special Publication, 1–26.

Bruce, M. E. C., Berg, R. R., Filz, G. M., Terashi, M., Yang, D. S. & Collin, J. G. (2013). Federal highway administration design manual: Deep mixing for embankment and foundation support. United States. Federal Highway Administation. Offices of Research & Development.

Cao, Y., Kurimoto, Y., Zhou, Y.-G., Ishikawa, A., & Chen, Y. (2023). Centrifuge model tests on liquefaction mitigation effect of soil-cement grids under large earthquake loadings. Bulletin of Earthquake Engineering, 21(9), 4217–4236.

Chen, T., & Guestrin, C. (2016). XGBoost: A scalable tree boosting system. Proceedings of the 22nd ACM SIGKDD International Conference on Knowledge Discovery and Data Mining, 785–794.

Filz, G., Adams, T., Navin, M., & Templeton, A. E. (2012). Design of deep mixing for support of levees and floodwalls. Grouting and Deep Mixing 2012, 89–133.

Filz, G. M., Hodges, D. K., Weatherby, D. E., & Marr, W. A. (2012). Standardized definitions and laboratory procedures for soil-cement specimens applicable to the wet method of deep mixing. 1–13.

Frikha, W., Zargayouna, H., Boussetta, S., & Bouassida, M. (2017). Experimental study of tunis soft soil improved by deep mixing column. Geotechnical and Geological Engineering, 35(3), 931–947.

Jamsawang, P., Boathong, P., Mairaing, W., & Jongpradist, P. (2016). Undrained creep failure of a drainage canal slope stabilized with deep cement mixing columns. Landslides, 13(5), 939–955.

Karpisz, I., Pyda, J., Cichy, L., & Sobala, D. (2018). Study of the effect of cement amount on the soil-cement sample strength. IOP Conference Series: Materials Science and Engineering, 365(4), 042061.

Kitazume, M., & Maruyama, K. (2007). Internal stability of group column type deep mixing improved ground under embankment loading. Soils and Foundations, 47(3), 437–455.

Lundberg, S. M., & Lee, S.-I. (2017). A unified approach to interpreting model predictions. In I. Guyon, U. V. Luxburg, S. Bengio, H. Wallach, R. Fergus, S. Vishwanathan, & R. Garnett (Eds.), Advances in Neural Information Processing Systems (Vol. 30). Curran Associates, Inc.

Martin, J. R., Olgun, C. G., Mitchell, J. K., & Durgunoglu, H. T. (2004). High-modulus columns for liquefaction mitigation. Journal of Geotechnical and Geoenvironmental Engineering, 130(6), 561–571.

Nenchev, B., Tao, Q., Dong, Z., Panwisawas, C., Li, H., Tao, B., & Dong, H. (2022). Evaluating data-driven algorithms for predicting mechanical properties with small datasets: A case study on gear steel hardenability. International Journal of Minerals, Metallurgy and Materials, 29(4), 836–847.

Pedregosa, F., Varoquaux, G., Gramfort, A., Michel, V., Thirion, B., Grisel, O., Blondel, M., Prettenhofer, P., Weiss, R., Dubourg, V., Vanderplas, J., Passos, A., Cournapeau, D., Brucher, M., Perrot, M., & Duchesnay, E. (2011). Scikit-learn: Machine learning in python. Journal of Machine Learning Research, 12, 2825–2830.

Pham, T. A., Koseki, J., & Dias, D. (2021). Optimum material ratio for improving the performance of cement-mixed soils. Transportation Geotechnics, 28, 100544.

Robertson, P. K. (2010). Soil behaviour type from the CPT: an update. 2nd International Symposium on Cone Penetration Testing, 2(56), 8.

Szymkiewicz, F., Barrett, A. G., Marino, J. P., Kouby, A. L., & Reiffsteck, P. (2015). Assessment of strength and other mechanical properties of the deep mixing material.

Zou, M., Jiang, W.-G., Qin, Q.-H., Liu, Y.-C., & Li, M.-L. (2022). Optimized XGBoost model with small dataset for predicting relative density of ti-6Al-4V parts manufactured by selective laser melting. Materials, 15(15), 5298.